Smectite formation in the presence of sulfuric acid: Implications for acidic smectite formation on early Mars

T.S. Peretyazhko[1*], P.B. Niles[2], B. Sutter[1], R. V. Morris[2], D. G. Agresti[3], L. Le[1], D.W. Ming[2]

[1] Jacobs, NASA Johnson Space Center, Houston, TX 77058

[2] NASA Johnson Space Center, Houston, TX 77058

[3] University of Alabama at Birmingham, Birmingham, AL 35294

Corresponding author: T. S. Peretyazhko, Jacobs, NASA Johnson Space Center, Houston, TX 77058 (tanya.peretyazhko@nasa.gov)

In preparation for

Geochimica et Cosmochimica Acta

Abstract

The excess of orbital detection of smectite deposits compared to carbonate deposits on the martian surface presents an enigma because smectite and carbonate formations are both favored alteration products of basalt under neutral to alkaline conditions. We propose that Mars experienced acidic events caused by sulfuric acid (H_2SO_4) that permitted phyllosilicate, but inhibited carbonate, formation. To experimentally verify this hypothesis, we report the first synthesis of smectite from Mars-analogue glass-rich basalt simulant (66 wt% glass, 32 wt% olivine, 2 wt% chromite) in the presence of H_2SO_4 under hydrothermal conditions (~200 °C). Smectites were analyzed by X-ray diffraction, Mössbauer spectroscopy, visible and near-infrared reflectance spectroscopy and electron microprobe to characterize mineralogy and chemical composition. Solution chemistry was determined by Inductively Coupled Plasma Mass Spectrometry. Basalt simulant suspensions in 11-42 mM H_2SO_4 were acidic with pH $\leq$ 2 at the beginning of incubation and varied from acidic (pH 1.8) to mildly alkaline (pH 8.4) at the end of incubation. Alteration of glass phase during reaction of the basalt simulant with H_2SO_4 led to formation of the dioctahedral smectite at final pH ~3 and trioctahedral smectite saponite at final pH ~4 and higher. Anhydrite and hematite formed in the final pH range from 1.8 to 8.4 while natroalunite was detected at pH 1.8. Hematite was precipitated as a result of oxidative dissolution of olivine present in Adirondack basalt simulant. Formation of secondary phases, including smectite, resulted in release of variable amounts of Si, Mg, Na and Ca while solubilization of Al and Fe was low. Comparison of mineralogical and solution chemistry data indicated that the type of smectite (i.e., dioctahedral vs trioctahedral) was likely controlled by Mg leaching from altering basalt and substantial Mg loss created favorable conditions for formation of dioctahedral smectite. We present a model for global-scale smectite formation on Mars via acid-sulfate conditions created by the volcanic outgassing of SO_2 in the Noachian and early Hesperian.

1. INTRODUCTION

Two global eras have been proposed to explain the observed mineralogy on Mars (Bibring et al., 2006). Abundant phyllosilicates dominated by the smectite group (nontronite, montmorillonite and saponite) were formed in the first era under water-rich neutral to alkaline conditions during the Noachian. Formation of sulfate-bearing phases occurred in the second era under acidic conditions likely caused by sulfuric acid during the Hesperian (Poulet et al., 2005; Bibring et al., 2006; Murchie et al., 2009; Bishop et al., 2013). However, such simplified pH-based division of aqueous history conflicts with some mineralogical observations. Large carbonate deposits together with phyllosilicates would be a characteristic of a Noachian Mars dominated by abundant liquid water, neutral/alkaline pH conditions, and a CO_2-rich atmosphere (Fairén et al., 2004), but mineralogical observations have detected only isolated carbonate deposits (Ehlmann et al., 2008; Milliken et al., 2009; Morris et al., 2010; Wray et al., 2016). The absence of widespread carbonate deposits could result from carbonate deposition on early Mars followed by its decomposition in acidic environments during Hesperian epoch (Fairén et al., 2004; Bibring et al., 2006; Chevrier et al., 2007). Alternatively, abundant carbonates may never have formed on early Mars because of short-term stability of liquid water and/or lack of dense CO_2 atmosphere during Noachian epoch (Bibring et al., 2006; Chevrier et al., 2007; Niles et al., 2013; Edwards and Ehlmann, 2015; Zolotov and Mironenko, 2016). Acidic events could also explain the apparent lack of abundant carbonate/phyllosilicate associations, because carbonate minerals do not form at acidic pH<6 conditions (Fairén et al., 2004; Fairén, 2013; Peretyazhko et al., 2016; Zolotov and Mironenko, 2016). The carbonate/smectite mineralogical observation might indicate that early Mars was not exclusively neutral-to-alkaline in pH but experienced

local and perhaps widespread acidic events. As a result, smectite formation on Mars could occur not only under commonly expected neutral/alkaline conditions but also in acidic environments.

In terrestrial environments smectites formed under acidic conditions have been reported in acidic saline lakes, seafloor hydrothermal vents and fumarolic areas (Haymon and Kastner, 1986; Story et al., 2010; Hynek et al., 2013). Limited laboratory observations have revealed smectite formation through hydrothermal basalt alteration in acidic pH 3-6 environments (Berger et al., 1987; Ghiara et al., 1993; Abdelouas et al., 1997; Dehouck et al., 2014). We have demonstated formation of saponite through alteration of Mars-analogue glass-rich basalt simulant in hydrothermal oxic and anoxic systems buffered by acetic acid (200 °C, pH_{RT} ~4 pH measured at room temperature, (Peretyazhko et al., 2016)).

The source of acidity on early Mars remains a subject for discussion. Two major acidity sources have been proposed for early Mars: (1) Fe(II) oxidative hydrolysis (Tosca et al., 2008; Hurowitz et al., 2010), and (2) volcanic release of sulfur dioxide, SO_2 (Zolotov and Mironenko, 2007; Berger et al., 2009; Gaillard and Scaillet, 2009; Righter et al., 2009; Gaillard et al., 2013; Zolotov and Mironenko, 2016). We have previously hypothesized that sulfuric acid (H_2SO_4) produced by volcanic SO_2 degassing on early Mars was the major source of acidity for the alteration of basaltic materials and subsequent formation of smectite (Peretyazhko et al., 2016). Our hypothesis was supported by modeling and mineralogical observations. For instance, recent detection of smectite minerals co-existing with sulfates might indicate that basalt weathering and smectite formation occurred under acidic conditions caused by sulfuric acid (Farrand et al., 2009; Wray et al., 2011; Cavanagh et al., 2015; Flahaut et al., 2015; Rampe et al., 2017). Thermodynamic modeling of basalt interaction with H_2SO_4-rich solutions revealed formation of Al-rich phyllosilicates (kaolinite, montmorillonite) under mildly acidic conditions followed by Mg/Fe smectites at higher pH (Zolotov and Mironenko, 2007; Zolotov and Mironenko, 2016)

and modelling of Mars-like aqueous systems predicted coexistence of smectite and sulfate minerals under mildly acidic pH 4-6 conditions (Fairén, 2013).

Formation of smectite through basalt alteration under Mars-relevant acid sulfate conditions has not been experimentally studied and the effect of pH and the nature of forming phyllosilicate minerals remains unknown. The objective of this work was to investigate formation of smectite through hydrothermal alteration of Mars-analogue basalt in the presence of sulfuric acid of variable concentrations, to assess acidity sources and to determine the extent to which H_2SO_4 is the source of acidity on early Mars.

2. MATERIALS AND METHODS

2.1. Synthesis and characterization of Adirondack basalt simulant

Synthetic basalt simulant of composition similar to that for Adirondack class rocks analyzed by the Mars Exploration Rover *Spirit* at Gusev Crater (McSween et al., 2006) was used in smectite formation studies (hereafter, denoted as Adirondack basalt simulant). The detailed synthesis procedure of the Adirondack basalt simulant is reported by Peretyazhko et al., (2016). Briefly, a powdered mixture of reagent-grade oxides and carbonates was melted at 1400 °C in an Au-Pt alloy crucible for 3d under the oxygen fugacity IW+1 (IW = iron-wüstite buffer) and quenched in water. The glassy product was then crushed, ground and sieved to <53 μm particle diameter for characterization and smectite formation experiments. X-ray diffraction analysis revealed that Adirondack simulant contained 66 wt% X-ray amorphous glass, 32 wt% olivine and 2 wt% chromite quench crystals within the glass matrix (Peretyazhko et al., 2016). Composition of the glass phase, olivine and chromite are summarized in Table EA-1.

2.2. Hydrothermal smectite formation experiments and characterization

Adirondack basalt simulant suspensions of 17 g/l (water to rock ratio = 60) were prepared by mixing 250 mg simulant with 15 ml of solutions having variable H_2SO_4 concentrations (11.0 ± 0.1 mM, 13.6 ± 0.1 mM, 16.3 ± 0.1 mM, 21.9 ± 0.1 mM, 30.6 ± 0.3 mM and 42.5 ± 0.2 mM). Initial sulfuric acid concentrations were measured as total sulfate by ion chromatography as described below. Duplicate samples were placed in batch reactors (Teflon lined 23 ml Parr acid digestion vessel) and incubated in an oven at 200 °C for 14d. The temperature of 200 °C was chosen because hydrothermal conditions are favorable for smectite formation promoting breaking of chemical bonds and rapid basalt alteration (Berger et al., 2014). However, smectite formation through alteration of basalts has been shown to occur at lower temperatures (Seyfried et al., 1978; McMurtry and Yeh, 1981; Kloprogge et al., 1999; Hynek et al., 2013). Sample preparation and hydrothermal incubation were performed under ambient atmosphere (oxidizing conditions). Our previous study (Peretyazhko et al., 2016) demonstrated that smectite formed through alteration of Adirondack basalt simulant under oxidizing and reducing acidic hydrothermal conditions and that oxidizing conditions only affected Fe oxidation state in smectite.

Suspension pH was measured immediately after mixing Adirondack basalt simulant with H_2SO_4 (pH_{0d}) and after opening the reactors at the end of 14d incubation (pH_{14d}) with AccupHast pH electrode using Orion Star A329 meter. Both measurements were performed at room temperature (RT) of ~25 ºC. After pH measurement, solution was collected in a syringe and passed through a 0.2 µm syringe filter (PVDF, Fisherbrand). An aliquot of each filtered solution was acidified with ultra-pure HNO_3 (Fisher) for dissolved Ca, Mg, Na, Si, Al and Fe analysis by Inductively Coupled Plasma Mass Spectrometry (ICP-MS, Element XR Thermo Scientific) with argon as the carrier gas. The remaining solution was analyzed for sulfate by ion chromatography

using Dionex ICS-2000 equipped with Dionex IonPac AS18 column (4 x 250 mm), Dionex EGC III KOH eluent and a suppressed conductivity detector Dionex AERS 500 4 mm with a 20 µm injection volume.

Separated solids were dried in an oven at 40 °C for ~1h prior to analysis. X-ray diffraction (XRD) patterns were recorded using a Panalytical X'Pert Pro with Co Kα radiation. Samples were analyzed at 45 kV/40 mA with a 0.02° 2θ step for 1 min. Programmable divergent and antiscatter slits were set to 1/4° with manual 1/2° antiscatter slit. The instrument was operated under ambient conditions and calibrated with novaculite (quartz) standard (Gemdugout, State College, PA). Standard powder mounts and low background silicon holders were used for analyses of bulk samples and clay size fractions, respectively. Clay size fractions were separated by ultrasonic dispersion (Kachanoski et al., 1988). Smectite-containing suspensions were ultrasonically treated with a probe-type sonicator (Soniprep 150) for 10s. The suspension was then allowed to sediment by gravity for ~1hr and supernatant containing the clay size fraction was collected. The procedure was repeated until supernatant solutions became clear and the collected clay fraction was separated by centrifugation. The clay fraction slurry was spread over the low background holder with a pipette and dried at RT prior to analysis. Clay fractions were treated with glycerol and KCl in order to confirm formation of smectite (Whittig and Allardice, 1986).

Visible and near-infrared reflectance (VNIR) spectra (0.35-2.5 µm) were measured with an Analytical Spectral Devices FieldSpec3 fiber-optic based spectrometer with a reflectance probe attachment (internal light source). Spectra were collected in absolute reflectance mode using a Spectralon standard. Continuum removed spectra were obtained using ENVI software (ENvironment for Visualizing Images, Harris Geospatial Solutions).

Mössbauer analyses were performed at RT under ambient conditions using MIMOS-II instruments that are the laboratory equivalent of the instruments onboard the Mars Exploration Rovers [SPESI, Inc., (Klingelhoefer et al., 2003)]. Velocity calibration was carried out with the program MERView (Agresti et al., 2007) using the MIMOS-II differential signal and the spectrum for metallic Fe foil acquired at RT. Mössbauer parameters [center shift (CS) with respect to metallic Fe foil at RT, quadrupole splitting (QS), magnetic hyperfine field strength (B_{hf}), and subspectral areas (A)] were obtained with a least-squares fitting procedure using MERFit (Agresti and Gerakines, 2009). Reported values for A were converted to % Fe using the f-factor ratio, $f_{Fe(III)}/f_{Fe(II)} = 1.21$ (Morris et al., 1995). Uncertainty for CS, QS, and full width at half maximum (FWHM) was ± 0.02 mm/s and uncertainty for A was ± 2% absolute. The following constraints were used in the least squares fitting procedure. (1) For each doublet, the component peaks were constrained to have equal widths and areas. (2) Because of the low observed intensity of hematite sextets, values for CS and QS were fixed to literature values (e.g.,(Morris et al., 1985)), peak areas were constrained to 3 : x : 1 : 1 : x : 3, where x is variable and FWHM decreased symmetrically toward zero velocity with skewed Lorentzian lineshapes. Four representative samples were analyzed by Mössbauer spectroscopy covering the whole range of the final pH_{14d} values.

Electron microprobe analyses of polished sections of smectite-containing Adirondack basalt simulant were analyzed for elemental composition using a CAMECA SX-100 electron microprobe (Figure EA-1). Backscattered electron imaging and analyses were collected at an accelerating voltage of 15 kV and probe current of 20 nA with a spot size of 1 μm. Element concentrations were calibrated using University of Tokyo Oxides standards. All measurements were made under 20s peak counting and 10s background counting. Because of high water content in smectite, total elemental content was lower than 100% in all analyzed samples. Data

with totals ≥74 wt% were used for smectite formula calculation. Residual sulfur and phosphorous were considered as impurities and subtracted from the totals in formula calculations. All Si atoms were assigned to tetrahedral sites and the remaining tetrahedral sites were filled with Al (Al = 8-Si). The remaining Al atoms, Mg, Fe and minor Ti, Ni, Cr and Mn were assigned to the octahedral sites, while Na, Ca and K were assigned to interlayer sites (Bain and Smith, 1987).

2.3. Calculations of sulfur degassing on Mars

Crust production model and the amount of sulfur degassing from magma were used to determine the release of SO_2 during Noachian/Early Hesperian epoch on Mars and then to obtain the total amount of acidity (total amount of protons, H^+) produced from the oxidation of SO_2 to H_2SO_4.

First, a crust production model described by Hirschmann and Withers (2008) was used to calculate crust accumulation from early Noachian (~4.5 Ga) to late Amazonian (0 Ga). The model is based on assumptions that crust formation is proportional to the heat flow and that total crust production during 4.5 Ga is $654 \cdot 10^6$ km^3 as estimated by (Greeley and Schneid, 1991). The model is described by the equation:

$$\frac{dV}{dt} = ae^{-ct} + be^{-dt} \quad (1)$$

where variables are V (crust production) and t (time) and constants are a = $9.277 \cdot 10^5$ km^3, b = $2.385 \cdot 10^5$ km^3, c = $6 \cdot 10^{-3}$ Ma^{-1}, d = $3.98 \cdot 10^{-4}$ Ma^{-1} (Hirschmann and Withers, 2008). The calculated total crust production is shown in Figure EA-2. The amount of sulfur released from magma was then calculated as

$$\text{Total } S = S_{magma}\, \rho\, V \quad (2)$$

where ρ is an average basalt density of 2800 kg/m^3 and S_{magma} is the amount of sulfur degassed from magma of 2400 mg/kg (Righter et al., 2009).

3. RESULTS

3.1. pH before and after incubation

Different initial H_2SO_4 concentrations led to variable degrees of basalt neutralization after 14d incubation. The average initial pH for all experiments was acidic ($pH_{0d} \leq 2$), and the final pH_{14d} varied over a wide range including acidic (pH_{14d} 1.8 and 2.2), moderately acidic (pH_{14d} 3.1 and 3.7), neutral (pH_{14d} 7.2) and slightly alkaline (pH_{14d} 8.4) (Figure 1).

3.2. Mineralogical characterization

3.2.1. X-ray diffraction

Powder XRD analyses of reaction products showed increasing phyllosilicate formation at $pH_{14d} \geq 3$ on the basis of increasing intensity of the 001 diffraction peak at ~15 Å while no phyllosilicate formation occurred at pH_{14d} 1.8 and 2.2 (Figure 2a, Table 1). After separation of the clay size fraction, the phyllosilicate was identified as smectite based on expansion of the 001 peak to 17.4-18 Å after glycerol treatment, its collapse to 12.8 Å at room temperature upon KCl addition, and its additional collapse to 10.1 Å after heating at 550 °C (Figure EA-3). The positions of 02*l* and 060 d-spacings allowed distinguishing dioctahedral from trioctahedral smectite (Moore and Reynolds, 1997; Vaniman et al., 2014). The 02*l* and 060 d-spacings revealed that trioctahedral smectite formed at pH_{14d} 3.7, 7.2 and 8.4 and the peak positions (Figure 2b, Table 2) were within the range reported for saponite (02*l*: 4.52-4.64 Å and 060: 1.53-1.56 Å (Treiman et al., 2014; Chemtob et al., 2015; Peretyazhko et al., 2016)). The 02*l* and 060 d-spacings at 4.48 Å and 1.50 Å, respectively, indicated formation of dioctahedral smectite at

248 pH_{14d} 3.1 (Figure 2b, Table 2). The peak positions were in agreement with d-spacing reported for
249 montmorillonite (02*l*: 4.47 Å and 060: 1.492-1.504 Å, (Moore and Reynolds, 1997; Vaniman et
250 al., 2014)). However, formation of montmorillonite could not be confirmed with VNIR and
251 electron microprobe analyses (sections 3.2.3 and 3.2.4) and therefore phyllosilicate formed in the
252 pH_{14d} 3.1 sample is referred as dioctahedral smectite. Formation of smectite in all samples was
253 accompanied by decrease in intensity of the broad basaltic glass peak between 20° and 40° 2θ
254 with respect to the unaltered material (Figure 2a) suggesting glass as the smectite progenitor.
255 Anhydrite ($CaSO_4$) was found to precipitate at all values of pH_{14d} and natroalunite
256 ($NaAl_3(SO_4)_2(OH)_6$) was detected only at pH_{14d} 1.8 (Figure 2a, Table 1). A weak diffraction
257 peak of hematite (α-Fe_2O_3) was observed in the pH_{14d} 1.8 sample (Figure 2a, Table 1), and the
258 presence of hematite was confirmed by Mössbauer spectroscopy (Section 3.2.2). Hematite was
259 not detected in any other samples by XRD, but Mössbauer analysis showed that hematite was
260 present in the pH_{14d} range from 1.8 to 8.4 (Section 3.2.2). Chromite, present in the unaltered
261 material, did not dissolve during incubation while olivine completely dissolved in the pH_{14d} 1.8
262 and 2.2 samples as evident from the disappearance of its sharp diffraction peaks (Figure 2a,
263 Table 1).
264 *3.2.2. Mössbauer spectroscopy*
265 Mössbauer analysis of unaltered Adirondack basalt simulant showed that Fe was
266 associated with olivine and glass phases, 19 ± 2 and 81 ± 2% respectively and was mostly Fe(II)
267 (Table EA-2, (Peretyazhko et al., 2016)).
268 Analysis of altered Adirondack basalt simulant revealed formation of smectite through
269 alteration of the glass phase. The decrease in the concentration of total Fe associated with the
270 glass phase (39 ± 2% pH_{14d} 3.1, 43 ± 2% pH_{14d} 3.7 and 54 ± 2% pH_{14d} 8.4, Figure 3a-c, Table
271 EA-2) compared to the unaltered simulant, was equal within error to amount of total Fe

associated with the smectite formed after 14d incubation (38 ± 2% pH_{14d} 3.1, 41 ± 2% pH_{14d} 3.7 and 56 ± 2% pH_{14d} 8.4, Figure 3a-c, Table EA-2). Smectite spectra were fit with one Fe(II) doublet (CS = 1.04 -1.09 mm/s and QS = 2.42 -2.66 mm/s) and one Fe(III) doublet (CS = 0.41 - 0.48 mm/s and QS = 0.54 - 0.70 mm/s QS, Table EA-2) and assigned to Fe(II) and Fe(III) in octahedral coordination (Treiman et al., 2014). The smectite was oxidized with Fe(III)/ΣFe equal to 0.61, 0.73 and 0.82 at pH_{14d} 3.1, 3.7 and 8.4, respectively.

The most acidic pH_{14d} 1.8 sample was also characterized by Fe(II) and Fe(III) doublets with parameters similar to those assigned to smectite in the other samples (Fe(II) doublet: CS = 1.03 mm/s and QS = 2.60 mm/s and Fe(III) doublet: CS = 0.46 mm/s and QS = 0.62 mm/s, Table EA-2). However, smectite did not form in this sample within XRD detection limits (Table 1). The Fe might be associated with an altered glass layer which forms during first stage of acidic basalt alteration (Berger et al., 1987; Oelkers, 2001) and/or with an incipient phyllosilicate with domains too small to coherently scatter X-rays.

The concentration of total Fe associated with olivine progressively decreased with decreasing pH_{14d}, and no Fe in olivine was detected in the pH_{14d} 1.8 sample as shown in Table EA-2. Olivine dissolution by acid-sulfate solutions could contribute Fe to smectite precipitation. However, the Mössbauer evidence is that Fe(II) from olivine dissolution was oxidized and precipitated as hematite, because the decrease in concentration of Fe(II) associated with olivine was associated with a concomitant increase in the concentration of Fe(III) associated with hematite (Figure 3, Table EA-2). Iron content in hematite (15 ± 2% pH_{14d} 1.8, 12 ± 2% pH_{14d} 3.1, 8 ± 2% pH_{14d} 3.7 and 2 ± 2% pH_{14d} 8.4, Figure 3, Table EA-2), was equal within an error of fitting to decrease in olivine Fe content with respect to the unaltered Adirondack basalt simulant (19 ± 2% pH_{14d} 1.8, 11 ± 3% pH_{14d} 3.1, 6 ± 3% pH_{14d} 3.7 and 4 ± 3% pH_{14d} 8.4, Figure 3, Table

EA-2). The hematite peaks were broad and skewed toward zero velocity, implying poor crystallinity (small particle diameter) and potentially Al substitution for Fe(III).

3.2.3. Smectite composition and structural formula

The structural formula calculated from electron microprobe analysis of smectite-containing particles (Table EA-3, Figure EA-1) showed that smectite contained Si and Al in tetrahedral layers, Al, Mg, Fe with traces of Ti, Mn, Ni and Cr in octahedral layers, and Na, Ca and K occupied interlayer sites. Given the high uncertainties in the measured data due to high water content in smectite, the results of electron microprobe analysis did not allow to accurately quantify smectite composition. Electron microprobe analysis indicated that smectite enriched in Fe and Mg formed at pH_{14d} 3.7, 7.2 and 8.4 while smectite equally enriched in Al, Mg and Fe formed at pH_{14d} 3.1 (Table EA-3). The average total number of octahedral cations in a unit cell was close to 6 in the pH_{14d} 3.7, 7.2 and 8.4 samples (Table EA-3) and was consistent with trioctahedral saponite. The total number of octahedral cations was close to 5 in the pH_{14d} 3.1 sample (Table EA-3) which might indicate formation of smectite containing dioctahedral and trioctahedral domains.

3.2.4. Visible and near-infrared spectroscopy

VNIR spectral features between ~1.2 and 2.5 μm (Figure 4, Table 2) for saponite formed at pH_{14d} 3.7, 7.2, and 8.4 were assigned to OH in H_2O and M-OH (~1.4 μm), to interlayer and adsorbed H_2O (~1.9 μm), and to trioctahedral M_3-OH and dioctahedral M_2-OH functional groups (2.2-2.5 μm), where M is any combination of Al, Mg, Fe(II) and Fe(III) as octahedral cations. The band centered between 2.30 and 2.32 μm was assigned to $(Mg, Fe(II), Fe(III))_3OH$ combination stretching and bending vibration (Neumann et al., 2011; Treiman et al., 2014). $(Mg, Fe(II), Fe(III))_3OH$ band center position was shifted to shorter wavelength in the pH_{14d} 8.4 sample with respect to the pH_{14d} 3.7 and 7.2 samples (Figure 4b, Table 2). The band position

shift could be due to increase in degree of Fe oxidation in saponite from Fe(III)/ΣFe = 0.73 at pH_{14d} 3.7 to Fe(III)/ΣFe = 0.82 at pH_{14d} 8.4, (Table EA-2, (Peretyazhko et al., 2016)). The position variability for the ~2.31 μm band might also result from heterogeneous distributions of cations on octahedral sites [e.g., $(Fe(III)_2Mg)$-OH versus $(Fe(III)Mg_2)$-OH]. Saponite observed at pH_{14d} 7.2 and 8.4 had a weaker band near 2.40 μm band commonly observed in Fe/Mg smectites (e.g., Carter et al., 2015; Chemtob et al., 2015). The exact band assignment is uncertain but might be due to $(Mg, Fe(II), Fe(III))_3OH$ combination stretching and translation vibration (Frost et al., 2002; Chemtob et al., 2015). The spectral feature near 2.24 μm was assigned to Al(Fe(III), Fe(II), Mg)OH (Madejová et al., 2011; Chemtob et al., 2015) and indicated the presence of octahedral Al, possibly present as dioctahedral domains as previously observed in synthetic saponite (Chemtob et al., 2015; Peretyazhko et al., 2016). Spectral properties of saponite synthesized at pH_{14d} 3.7, 7.2 and 8.4 were similar to the properties reported for smectite on Mars by VNIR spectrometers. The bands near 2.30 and 2.40 μm has been reported in Fe/Mg-smectite identified on Mars while the band at 2.24 μm is present in about 10% of Fe/Mg-phyllosilicate spectra (Carter et al., 2013), including nontronite (Bishop et al., 2013) but not saponite.

The spectrum of the pH_{14d} 3.1 sample containing dioctahedral smectite was similar to the spectra of the untreated Adirondack basalt simulant and pH_{14d} 1.8 and 2.2 samples (Figure 4b). All these samples had a broad band centered on 2.21-2.22 μm likely resulting from vibration of Si-OH associated with the unaltered glass phase. The diagnostic band of montmorillonite at 2.20 μm was not distinguishable from the basalt band because of relatively low smectite abundance at pH_{14d} 3.1 (indicative by low intensity 001 diffraction peak in the sample, Figure 2a).

Hematite presence was evident from the ferric absorption edge between ~0.50 um and ~0.75 um (Figure 4a) corresponding to the onset of strong absorption and a relative reflectivity maximum for hematite (Morris et al., 1985). The VNIR manifestation of the hematite was most

noticeable for the pH_{14d} 1.8 sample which had the highest hematite content (15% of total Fe, Table EA-2)

3.3. Characterization of aqueous phase

Mineralogical transformations of Adirondack basalt simulant to smectite, anhydrite, hematite and natroalunite (Table 1) resulted in release of variable proportions of Si, Mg, Na and Ca. Complete dissolution of olivine in the pH_{14d} 1.8 and 2.2 samples and subsequent release of Mg and Si into solution (Figure 5a) were lower than the expected Si and Mg concentrations if all olivine was dissolved (32 ± 3 mM Si and 42 ± 4 mM Mg based on the total SiO_2 and MgO contents in olivine, Table EA-1). The results suggest that Si and Mg dissolved from olivine were partially incorporated into an altered glass phase under acidic conditions (Berger et al., 1987).

Smectite formation in the pH_{14d} range from 3.1 to 8.4 (Figure 2a) led to decrease in Si and Mg dissolution (Figure 5a) where the Mg dissolution likely controlled the nature of the forming smectite mineral (Meunier, 2005). Dioctahedral smectite was only detected in the pH_{14d} 3.1 sample in which nearly 50% of the total Mg was leached into solution (calculations are based on dissolved Mg concentrations in Figure 5a and total MgO in the glass phase, Table EA-1) while formation of trioctahedral saponite (pH_{14d} 3.7, 7.2 and 8.4) was accompanied by lower or no Mg release into solution.

Dissolved Na was affected by precipitation of natroalunite and smectite formation. Dissolved Na concentration was low and did not change in the pH_{14d} range from 1.8 to 3.1 then increased as pH shifted from acidic to slightly alkaline (Figure 5b). Low release of Na from basaltic glass at pH_{14d} 1.8-3.1 could result from precipitation of natroalunite, although the presence of this phase was only confirmed at pH_{14d} 1.8 (Table 1). Dissolved Na increased in the pH_{14d} range from 3.1 to 8.4 (Figure 5b) due to Na loss from glass phase during alteration of Adirondack basalt simulant into smectite (Peretyazhko et al., 2016). Similar to Na, Ca was

expected to increase in solution with increasing basalt alteration as pH rose (Berger et al., 1987). However, dissolved Ca concentration did not change (Figure 5b), and such non-pH-dependent Ca release, together with the observed decrease in sulfate concentration (Figure 5c), resulted from anhydrite precipitation (Figure 2a, Table 1) which is favorable at elevated temperatures (Bishop et al., 2014).

Solution concentrations of Al and Fe were low for all samples resulting from their incorporation into secondary phases (Figure EA-4, Tables 1 and 2). Dissolved Al did not exceed 0.04 mM (Figure EA-4a) as a result of precipitation of natroalunite at pH_{14d} 1.8, low release from glass alteration and incorporation into smectite at higher pH values (Tables 2 and EA-3) and potentially in hematite. Dissolved Fe was <0.15 mM (Figure EA-4b) in all samples due to precipitation of hematite accompanying olivine dissolution (Figure 3), low release from altering glass phase and smectite formation (Tables 2 and EA-3).

4. DISCUSSION

The formation of smectite in the Noachian and early Hesperian has been attributed to aqueous alteration of basaltic materials under neutral to alkaline pH aqueous conditions (Bibring et al., 2006; Chevrier et al., 2007; Ehlmann et al., 2009; Bishop et al., 2013; Bristow et al., 2015; Flahaut et al., 2015; Jain and Chauhan, 2015). However, the results of our experiments show that formation of smectite from Mars-analogue basalt simulant is possible in much more acidic environments. We found that gradual acid neutralization during acid-sulfate alteration of the basalt simulant under hydrothermal conditions led to smectite formation at $pH_{14d} \geq 3$. The nature of the forming smectite mineral varied with the solution final pH. Dioctahedral smectite equally

enriched in Al, Fe and Mg formed at pH_{14d} ~3 followed by saponite enriched in Fe and Mg at pH_{14d} close to 4 or higher.

Our experimental results demonstrate that smectite formation through basalt alteration on Mars was not limited to neutral/alkaline pH conditions but could partially occur under acidic conditions once solution pH was close to 3 or higher. Sources of acidity on early Mars and the persistence of acidic aqueous environments have been controversial. The basaltic crust should provide enormous acid neutralizing potential (Niles and Michalski, 2009) suggesting that aqueous systems on Mars should be largely alkaline. However, as noted above, absence of large scale carbonate deposits shows an evidence for acidic conditions even in heavily altered regions of the martian crust (Fairén et al., 2004). The principal acidity sources proposed for early Mars are Fe(II) oxidative hydrolysis (Tosca et al., 2008; Hurowitz et al., 2010) and SO_2 degassing (Berger et al., 2009; Gaillard and Scaillet, 2009; Righter et al., 2009; Gaillard et al., 2013). We argue here that SO_2 degassing was the major source of acidity on early Mars generating H_2SO_4 sufficient for acidic phyllosilicate formation through basalt alteration and Fe(II) oxidative hydrolysis (i.e., Fe(III) hydrolysis) was likely not the source of wide-spread acidity on Mars.

4.1. Acidity sources on early Mars: Fe(II) oxidative hydrolysis

Iron(III) hydrolysis was first suggested as the source of acidity at Meridiani Planum (Hurowitz et al., 2010) and was further generalized as a possible widespread acidity source on early Mars (e.g., (Ehlmann et al., 2011; Bowen et al., 2012; Horgan and Bell III, 2012; McLennan, 2012; Marlow et al., 2014; Kaplan et al., 2016)). The Fe(II) oxidative hydrolysis model proposed that upwelling of anoxic Fe(II)-containing groundwater generated from basalt dissolution under anoxic circum-neutral pH conditions could lead to surface oxidation of Fe(II) to Fe(III) followed by Fe(III) hydrolysis, release of H^+ and precipitation of Fe(III) secondary

minerals (Hurowitz et al., 2010). The latter include nanophase iron(III) (hydr)oxides (interpreted as schwertmannite ($FeO(OH)_{0.75}(SO_4)_{0.125}$) (Hurowitz et al., 2010)), jarosite ($(K,Na)Fe_3(SO_4)_2(OH)_6$) and hematite (α-Fe_2O_3) detected by Mössbauer spectroscopy at Meridiani Planum (Morris et al., 2006). The reactions below summarize the mechanism proposed for acidity generation following the sequence developed by Hurowitz et al., (2010) with the exception that eq. 3 is included for basalt dissolution (eq. 3 written for olivine Fe(II)-end member fayalite (Fe_2SiO_4)):

$$0.5Fe_2SiO_4 + 2H^+ \rightarrow Fe^{2+} + 0.5SiO_2 + H_2O \text{ or} \quad (3a)$$

$$0.5Fe_2SiO_4 + H_2O \rightarrow Fe^{2+} + 0.5SiO_2 + 2OH^- \quad (3b)$$

$$Fe^{2+} + 0.25O_2 + H^+ \rightarrow Fe^{3+} + 0.5H_2O \quad (4)$$

$$Fe^{3+} + 0.125SO_4^{2-} + 1.75H_2O \rightarrow FeO(OH)_{0.75}(SO_4)_{0.125} + 2.75H^+ \quad (5)$$

$$FeO(OH)_{0.75}(SO_4)_{0.125} + 0.25H_2O + 0.75H^+ + 0.5417SO_4^{2-} + 0.33(K^+ \text{ or } Na^+) \rightarrow 0.33(K,Na)Fe_3(SO_4)_2(OH)_6 \quad (6)$$

$$FeO(OH)_{0.75}(SO_4)_{0.125} + 0.25H_2O \rightarrow FeOOH + 0.25H^+ + 0.125SO_4^{2-} \quad (7)$$

$$FeOOH \rightarrow 0.5Fe_2O_3 + 0.5H_2O \quad (8)$$

While groundwater interaction with basalt was suggested to be a source of dissolved Fe(II), basalt dissolution (eq. 3) was not included into Fe(II) oxidative hydrolysis model (Hurowitz et al., 2010). As a result, the model predicted that sufficient amount of H^+ was produced through Fe(III) hydrolysis to develop acidic conditions (Hurowitz et al., 2010). If basalt dissolution reactions are added to the model, then no acidity would be generated because Fe(II) release is accompanied by OH^- release (e.g., eq. 3b, Text EA-1). While our calculations only account for Fe, the release of Mg, Ca, and Na from the basalts will also be accompanied by release of OH^- which will contribute to generation of additional alkalinity.

The OH^- generated from dissolution of basalt (eq. 3) could be neutralized by H^+ produced through oxidative dissolution of Fe(II) sulfides present in basalt. However, the produced H^+ will not be sufficient to neutralize all released OH^- on the basis of current estimates of low abundances of Fe(II) sulfides in martian basalts (1600 mg/kg S in shergottite sulfides or 0.16 wt%, (Righter et al., 2009)). Alternatively, the OH^- released from basalt together with Fe(II), Mg, Ca and Na could be neutralized if the anoxic alkaline solutions encounter anoxic acidic solutions. If all released OH^- is neutralized, then Fe(II) oxidation followed by hydrolysis under oxic conditions will lead to development of acidic conditions according to the Hurowitz et al., (2010) model (eqs. 4-8). However, such scenario will require presence of acidic conditions, for instance H_2SO_4, before Fe(III) hydrolysis occurred.

4.2. Acidity sources on early Mars: SO_2 degassing and H_2SO_4 formation

Magmatic sulfur degassing was the dominant source for sulfates deposited on the surface of Mars (Righter et al., 2009), but was SO_2 release on early Mars able to generate the amount of H_2SO_4 sufficient for acidic phyllosilicate formation through alteration of basalt?

The calculated amount of sulfur release (eq. 2) during Noachian/early Hesperian epoch was 2.5×10^{21} g [~4.5 Ga - ~3.4 Ga; an intermediate value of 3.4 Ga was used for early Hesperian/Late Hesperian boundary which is around 3.2 Ga - 3.6 Ga (Hartmann, 2005); Figure 6]. If all sulfur was released as SO_2 and converted to H_2SO_4 then around 1.6×10^{20} moles of H^+ was produced during dissociation of all acid in water. Formation of sulfuric acid might occur through disproportionation of SO_2 to H_2SO_4 and elemental S and S could be further transformed into H_2SO_4 in the presence of oxidizing agent and water (Habashi and Bauer, 1966; Halevy et al., 2007). It should be noted, however, an assumption that all degassed sulfur was transformed into

sulfuric acid likely overestimates the amount of produced acidity but our calculations allows to potentially evaluate an upper limit of acidity that could have been generated on early Mars.

The protons generated from sulfuric acid are neutralized by Ca, Mg and Na in basalt via proton exchange leading first to formation of an altered hydrated silica layer enriched in Fe and Al (Berger et al., 1987; Peretyazhko et al., 2016) by schematic reactions:

$$\text{Na-basalt} + H^+ = \text{H-basalt} + Na^+ \quad (9)$$

$$\text{Ca-basalt} + 2H^+ = \text{2H-basalt} + Ca^{2+} \quad (10)$$

$$\text{Mg-basalt} + 2H^+ = \text{2H-basalt} + Mg^{2+} \quad (11)$$

Crystallization of phyllosilicate from an altered layer does not substantially change pH as shown in the previous studies of smectite formation through basalt alteration (Ghiara et al., 1993; De La Fuente et al., 2002; Peretyazhko et al., 2016). Iron was not included into calculations because overall process including dissolution of olivine followed by Fe(II) oxidation, Fe(III) hydrolysis and hematite precipitation (Table 1) does not produce or consume H^+ (Text EA-1). Approximately 9.4 mol_{H+}/kg_{basalt} H^+ is required for complete neutralization of Na, Ca and Mg in basalt of Adirondack composition (Text EA-2). The amount of H^+ generated from volcanic outgassing of SO_2 ($1.6x10^{20}$ moles) during the Noachian and Hesperian would be sufficient for neutralization of Ca, Mg and Na along with phyllosilicate formation in a 42 m thick basalt layer over the entire planet (Text EA-3). Given that formation of smectite requires Mg to be present in the altering basalt (Kloprogge et al., 1999), partial H^+ neutralization by cations would be a more realistic scenario on Mars. Noachian-aged terrains such as Mawrth Vallis have been estimated to contain 20-65% smectite (Poulet et al., 2008). Assuming that the smectite abundance in Mawrth Vallis is representative of H^+ neutralization and, consequently, degree of basalt alteration in ancient martian terrains, the calculated average global depth of basaltic alteration would be between 60 m (65% smectite content) to 200 m (20% smectite content) on the entire planet under

the constraint that alteration of 42 m thick basalt leads to 100% neutralization of Na, Ca and Mg. The calculated depth range is consistent with phyllosilicate layer thickness of a few hundreds of meters estimated in Noachian-aged terrains (Loizeau et al., 2012). Our acidity calculations and experimental results, therefore, provide evidence that SO_2 degassing would result in production of large amounts of H^+ and gradual neutralization of sulfuric acid during basalt alteration could be an important mechanism of smectite formation on early Mars.

5. SIGNIFICANCE AND CONCLUSIONS

Our experiments demonstrated formation of smectite through hydrothermal acid-sulfate alteration of Mars-analogue glass-rich basalt (66 wt% glass, 32 wt% olivine and 2 wt% chromite). Basalt simulant suspensions were acidic with initial $pH_{0d} \leq 2$ while final pH_{14d} varied from acidic to mildly alkaline (pH_{14d} 1.8-8.4) at the end of 14d incubation at 200 ºC. Alteration of the glass phase of basalt simulant resulted in formation of dioctahedral smectite as pH_{14d} reached ~3 followed by trioctahedral saponite at pH_{14d} close to 4 or higher. Reaction of Adirondack basalt simulant with sulfuric acid also led to formation of anhydrite at all pH_{14d} values while natroalunite was detected at pH_{14d} 1.8. Hematite precipitated as a result of partial or complete oxidative dissolution of olivine in the pH_{14d} range from 1.8 to 8.4.

Acidity on early Mars can be accounted for by volcanic outgassing of SO_2 and formation of sulfuric acid. Acid-sulfate conditions, suitable enough to form smectite and prevent carbonate formation were likely sustained by low water/rock ratio and short duration of water-rock interaction (Berger et al., 2009; Berger et al., 2014). Acidic smectite formation areas on early Mars might be constrained to near-surface hydrothermal areas with magmatic outgassing resulted from volcanic or impact activity (Solomon et al., 2005; Hynek et al., 2013). In these

systems only small portions of crust are exposed to acidity generated by H_2SO_4 formed from degassed SO_2. Short-term aquatic systems analogous to ephemeral acid saline lakes in Western Australia might also allow development of acidic conditions (Story et al., 2010; Bowen et al., 2012). Although there may also be acidity generated by the Fe(II) oxidative hydrolysis in local environments, our calculations indicate that this mechanism is not a plausible large-scale acidity source because of the alkalinity that is generated during basalt dissolution.

Formation of phyllosilicate by sulfuric acid alteration of basaltic materials on Mars would likely be accompanied by precipitation of sulfate minerals including anhydrite. Although anhydrite cannot be detected by the same remote sensing measurements used to detect phyllosilicates because of the absence of diagnostic H_2O spectral features in the VNIR, anhydrite might coprecipitate with phyllosilicate in deposits formed under hydrothermal sulfuric acid environments (>60 °C (Bishop et al., 2014)). Acid-sulfate smectite formation might also occur in younger terrains. Phyllosilicates (e.g., smectite) co-existing with anhydrite in Gale crater may have formed along with the anhydrite under acid sulfate conditions (Rampe et al., 2017). The hypothesis is supported by occurrence of jarosite in these mudstones in Gale crater indicative of acidic environments (Rampe et al., 2017). Fe/Mg-rich phyllosilicates interbedded with sulfate minerals in Meridiani Planum have been proposed to form prior to sulfates in moderate pH, sulfate-free aqueous environments followed by sulfate precipitation from acidic surface and groundwater (Flahaut et al., 2015). Our findings demonstrate that multiple events are not required to form interbedded phyllosilicates and sulfates deposits. Acid-sulfate alteration can explain martian mineralogical observations including mixed phyllosilicate/sulfate deposits and lack of abundant carbonate deposits.

ACKNOWLEDGEMENTS

We thank Z. Peng for performing ICP-MS analysis. We thank Dr. Cuardos, Dr. Zolotov and two anonymous reviewers for valuable suggestions and comments that help to improve the quality of the manuscript. We thank the Associate Editor Dr. Catalano for handling the manuscript.This work was supported by NASA's Mars Fundamental Research Program grant # 11-MFRP11-0090.

REFERENCES

Abdelouas A., Crovisier J.-L., Lutze W., Grambow B., Dran J.-C. and Müller R. (1997) Surface layers on a borosilicate nuclear waste glass corroded in $MgCl_2$ solution. *J. Nucl. Mater.* **240**, 100-111.

Agresti D. G., Dyar M. D. and Schaefer M. W. (2007) Velocity scales for Mars Mössbauer data. *NASSAU 2006,* 67-74.

Agresti D. G. and Gerakines P. A. (2009) Simultaneous fitting of Mars Mössbauer data. *ICAME 2007,* 1347-1354.

Bain D. C. and Smith B. F. L. (1987) Chemical analysis, In: *A handbook of determinative methods in clay mineralogy* (ed. M. J. Wilson). Chapman and Hall, New York, pp. 248-275.

Berger G., Meunier A. and Beaufort D. (2014) Clay mineral formation on Mars: Chemical constraints and possible contribution of basalt out-gassing. *Planet. Space Sci.* **95**, 25-32.

Berger G., Schott J. and Loubet M. (1987) Fundamental processes controlling the first stage of alteration of a basalt glass by seawater: an experimental study between 200 and 320 C. *Earth. Planet. Sci. Lett.* **84**, 431-445.

Berger G., Toplis M. J., Treguier E., d'Uston C. and Pinet P. (2009) Evidence in favor of small amounts of ephemeral and transient water during alteration at Meridiani Planum, Mars. *Am. Mineral.* **94**, 1279-1282.

575 Bibring J.-P., Langevin Y., Mustard J. F., Poulet F., Arvidson R., Gendrin A., Gondet B.,
576 Mangold N., Pinet P. and Forget F. (2006) Global mineralogical and aqueous Mars history
577 derived from OMEGA/Mars Express data. *Science* **312**, 400-404.

578 Bishop J. L., Lane M. D., Dyar M. D., King S. J., Brown A. J. and Swayze G. A. (2014) What
579 lurks in the martian rocks and soil? Investigations of sulfates, phosphates, and perchlorates.
580 Spectral properties of Ca-sulfates: gypsum, bassanite, and anhydrite. *Am. Mineral.* **99**, 2105-
581 2115.

582 Bishop J. L., Loizeau D., McKeown N. K., Saper L., Dyar M. D., Des Marais D. J., Parente M.
583 and Murchie S. L. (2013) What the ancient phyllosilicates at Mawrth Vallis can tell us about
584 possible habitability on early Mars. *Planet. Space Sci.* **86**, 130-149.

585 Bowen B. B., Benison K. C. and Story S. (2012) Early diagenesis by modern acid brines in
586 Western Australia and implications for the history of sedimentary modification on Mars. *Mars*
587 *Sedimentology, SEPM Special Publication* **102**, 229-252.

588 Bristow T. F., Bish D. L., Vaniman D. T., Morris R. V., Blake D. F., Grotzinger J. P., Rampe E.
589 B., Crisp J. A., Achilles C. N. and Ming D. W. (2015) The origin and implications of clay
590 minerals from Yellowknife Bay, Gale crater, Mars. *Am. Mineral.* **100**, 824-836.

591 Carter J., Poulet F., Bibring J. P., Mangold N. and Murchie S. (2013) Hydrous minerals on Mars
592 as seen by the CRISM and OMEGA imaging spectrometers: Updated global view. *J. Geophys.*
593 *Res. Planets* **118**, 831-858.

Cavanagh P. D., Bish D. L., Blake D. F., Vaniman D. T., Morris R. V., Ming D. W., Rampe E. B., Achilles C. N., Chipera S. J., Treiman A. H., Downs R. T. and Morrison S. M. (2015) Confidence Hills mineralogy and CheMin results from base of Mt. Sharp, Pahrump Hills, Gale Crater, Mars LPSC.

Chemtob S. M., Nickerson R. D., Morris R. V., Agresti D. G. and Catalano J. G. (2015) Synthesis and structural characterization of ferrous trioctahedral smectites: Implications for clay mineral genesis and detectability on Mars. *J.Geophys. Res. Planets*. **120**, 1119 -1140

Chevrier V., Poulet F. and Bibring J.-P. (2007) Early geochemical environment of Mars as determined from thermodynamics of phyllosilicates. *Nature* **448**, 60-63.

Craddock R. A. and Greeley R. (2009) Minimum estimates of the amount and timing of gases released into the martian atmosphere from volcanic eruptions. *Icarus* **204**, 512-526.

De La Fuente S., Cuadros J. and Linares J. (2002) Early stages of volcanic tuff alteration in hydrothermal experiments: formation of mixed-layer illite-smectite. *Clays Clay Miner.* **50**, 578-590.

Dehouck E., Gaudin A., Mangold N., Lajaunie L., Dauzères A., Grauby O. and Le Menn E. (2014) Weathering of olivine under CO_2 atmosphere: a martian perspective. *Geochim. Cosmochim. Acta* **135**, 170-189.

Edwards C. S. and Ehlmann B. L. (2015) Carbon sequestration on Mars. *Geo* **43**, 863-866.

612 Ehlmann B. L., Mustard J. F., Murchie S. L., Bibring J.-P., Meunier A., Fraeman A. A. and
613 Langevin Y. (2011) Subsurface water and clay mineral formation during the early history of
614 Mars. *Nature* **479**, 53-60.

615 Ehlmann B. L., Mustard J. F., Murchie S. L., Poulet F., Bishop J. L., Brown A. J., Calvin W. M.,
616 Clark R. N., Des Marais D. J. and Milliken R. E. (2008) Orbital identification of carbonate-
617 bearing rocks on Mars. *Science* **322**, 1828-1832.

618 Ehlmann B. L., Mustard J. F., Swayze G. A., Clark R. N., Bishop J. L., Poulet F., Des Marais D.
619 J., Roach L. H., Milliken R. E. and Wray J. J. (2009) Identification of hydrated silicate minerals
620 on Mars using MRO-CRISM: Geologic context near Nili Fossae and implications for aqueous
621 alteration. *J. Geophys. Res. Planets* **114**.

622 Fairén A. G. (2013) Coeval synthesis of cold aqueous mineralogies on Mars, In: *Mars: evolution,*
623 *geology and exploration* (ed. A. G. Fairén). Nova Science Publisher.

624 Fairén A. G., Fernández-Remolar D., Dohm J. M., Baker V. R. and Amils R. (2004) Inhibition
625 of carbonate synthesis in acidic oceans on early Mars. *Nature* **431**, 423-426.

626 Farrand W. H., Glotch T. D., Rice J. W., Hurowitz J. A. and Swayze G. A. (2009) Discovery of
627 jarosite within the Mawrth Vallis region of Mars: Implications for the geologic history of the
628 region. *Icarus* **204**, 478-488.

629 Flahaut J., Carter J., Poulet F., Bibring J.-P., van Westrenen W., Davies G. and Murchie S.
630 (2015) Embedded clays and sulfates in Meridiani Planum, Mars. *Icarus* **248**, 269-288.

631 Frost R. L., Kloprogge J. T. and Ding Z. (2002) Near-infrared spectroscopic study of nontronites
632 and ferruginous smectite. *Spectrochim. Acta* **58**, 1657-1668.

633 Gaillard F., Michalski J., Berger G., McLennan S. M. and Scaillet B. (2013) Geochemical
634 reservoirs and timing of sulfur cycling on Mars. *Space Sci. Rev.* **174**, 251-300.

635 Gaillard F. and Scaillet B. (2009) The sulfur content of volcanic gases on Mars. *Earth. Planet.*
636 *Sci. Lett.* **279**, 34-43.

637 Ghiara M., Franco E., Petti C., Stanzione D. and Valentino G. (1993) Hydrothermal interaction
638 between basaltic glass, deionized water and seawater. *Chem. Geol.* **104**, 125-138.

639 Greeley R. and Schneid B. (1991) Magma generation on Mars- Amounts, rates, and
640 comparisons with earth, moon, and Venus. *Science* **254**, 996-998.

641 Habashi F. and Bauer E. (1966) Aqueous oxidation of elemental sulfur. *Ind. Eng. Chem.*
642 *Fundam.* **5**, 469-471.

643 Halevy I., Zuber M. T. and Schrag D. P. (2007) A sulfur dioxide climate feedback on early
644 Mars. *Science* **318**, 1903-1907.

645 Hartmann W. K. (2005) Martian cratering 8: Isochron refinement and the chronology of Mars.
646 *Icarus* **174**, 294-320.

647 Haymon R. M. and Kastner M. (1986) The formation of high temperature clay minerals from
648 basalt alteration during hydrothermal discharge on the East Pacific Rise axis at 21 N. *Geochim.*
649 *Cosmochim. Acta* **50**, 1933-1939.

650 Hirschmann M. M. and Withers A. C. (2008) Ventilation of CO_2 from a reduced mantle and
651 consequences for the early Martian greenhouse. *Earth. Planet. Sci. Lett.* **270**, 147-155.

652 Horgan B. and Bell III J. F. (2012) Widespread weathered glass on the surface of Mars. *Geology*
653 **40**, 391-394.

654 Hurowitz J. A., Fischer W. W., Tosca N. J. and Milliken R. E. (2010) Origin of acidic surface
655 waters and the evolution of atmospheric chemistry on early Mars. *Nat. Geosci.***3**, 323-326.

656 Hynek B. M., McCollom T. M., Marcucci E. C., Brugman K. and Rogers K. L. (2013)
657 Assessment of environmental controls on acid-sulfate alteration at active volcanoes in
658 Nicaragua: Applications to relic hydrothermal systems on Mars. *J. Geophys. Res. Planets* **118**,
659 2083-2104.

660 Jain N. and Chauhan P. (2015) Study of phyllosilicates and carbonates from the Capri Chasma
661 region of Valles Marineris on Mars based on Mars Reconnaissance Orbiter-Compact
662 Reconnaissance Imaging Spectrometer for Mars (MRO-CRISM) observations. *Icarus* **250**, 7-17.

663 Kachanoski R., Voroney R. and Gregorich E. (1988) Ultrasonic dispersion of aggregates:
664 distribution of organic matter in size fractions. *Can. J. Soil. Sci.* **68**, 395-403.

665 Kaplan H. H., Milliken R. E., Fernández-Remolar D., Amils R., Robertson K. and Knoll A. H.
666 (2016) Orbital evidence for clay and acidic sulfate assemblages on Mars based on mineralogical
667 analogs from Rio Tinto, Spain. *Icarus* **275**, 45-64.

668 Klingelhoefer G., Morris R. V., Bernhardt B., Rodionov D., De Souza P., Squyres S., Foh J.,
669 Kankeleit E., Bonnes U. and Gellert R. (2003) Athena MIMOS II Mössbauer spectrometer
670 investigation. *J. Geophys. Res. Planets* **108**.

671 Kloprogge J. T., Komarneni S. and Amonette J. E. (1999) Synthesis of smectite clay minerals: a
672 critical review. *Clays Clay Miner.* **47**, 529-554.

673 Loizeau D., Werner S., Mangold N., Bibring J.-P. and Vago J. (2012) Chronology of deposition
674 and alteration in the Mawrth Vallis region, Mars. *Planet. Space Sci.* **72**, 31-43.

675 Madejová J., Balan E. and Petit S. (2011) Application of vibrational spectroscopy to the
676 characterization of phyllosilicates and other industrial minerals. *Advances in the*
677 *Characterization of Industrial Minerals: Notes in Mineralogy* **9**, 171-226.

678 Marlow J. J., LaRowe D. E., Ehlmann B. L., Amend J. P. and Orphan V. J. (2014) The potential
679 for biologically catalyzed anaerobic methane oxidation on ancient Mars. *Astrobiology* **14**, 292-
680 307.

681 McLennan S. M. (2012) Geochemistry of sedimentary processes on Mars. *Sediment. Geol.Mars*
682 **102**, 119-138.

683 McMurtry G. M. and Yeh H.-W. (1981) Hydrothermal clay mineral formation of East Pacific
684 Rise and Bauer Basin sediments. *Chem. Geol.* **32**, 189-205.

McSween H. Y., Wyatt M. B., Gellert R., Bell J., Morris R. V., Herkenhoff K. E., Crumpler L. S., Milam K. A., Stockstill K. R. and Tornabene L. L. (2006) Characterization and petrologic interpretation of olivine-rich basalts at Gusev Crater, Mars. *J. Geophys. Res. Planets* **111**.

Meunier A. (2005) *Clays*. Springer Science & Business Media.

Milliken R., Fischer W. and Hurowitz J. (2009) Missing salts on early Mars. *Geophys. Res. Lett.* **36**.

Moore D. M. and Reynolds R. C. J. (1997) *X-ray diffraction and the identification and analysis of clay minerals*. Oxford University Press, New York.

Morris R. V., Golden D., Bell J. F. and Lauer H. (1995) Hematite, pyroxene, and phyllosilicates on Mars: Implications from oxidized impact melt rocks from Manicouagan Crater, Quebec, Canada. *J. Geophys. Res. Planets* **100**, 5319-5328.

Morris R. V., Klingelhoefer G., Schröder C., Rodionov D. S., Yen A., Ming D. W., De Souza P., Wdowiak T., Fleischer I. and Gellert R. (2006) Mössbauer mineralogy of rock, soil, and dust at Meridiani Planum, Mars: Opportunity's journey across sulfate-rich outcrop, basaltic sand and dust, and hematite lag deposits. *J. Geophys. Res. Planets* **111**.

Morris R. V., Lauer H. V., Lawson C. A., Gibson E. K., Nace G. A. and Stewart C. (1985) Spectral and other physicochemical properties of submicron powders of hematite (α-Fe_2O_3), maghemite (γ-Fe_2O_3), magnetite (Fe_3O_4), goethite (α-FeOOH), and lepidocrocite (γ-FeOOH). *J. Geophys. Res. Solid Earth* **90**, 3126-3144.

704 Morris R. V., Ruff S. W., Gellert R., Ming D. W., Arvidson R. E., Clark B. C., Golden D.,
705 Siebach K., Klingelhöfer G. and Schröder C. (2010) Identification of carbonate-rich outcrops on
706 Mars by the Spirit rover. *Science* **329**, 421-424.

707 Murchie S. L., Mustard J. F., Ehlmann B. L., Milliken R. E., Bishop J. L., McKeown N. K., Noe
708 Dobrea E. Z., Seelos F. P., Buczkowski D. L. and Wiseman S. M. (2009) A synthesis of Martian
709 aqueous mineralogy after 1 Mars year of observations from the Mars Reconnaissance Orbiter. *J.*
710 *Geophys. Res. Planets* **114**.

711 Neumann A., Petit S. and Hofstetter T. B. (2011) Evaluation of redox-active iron sites in
712 smectites using middle and near infrared spectroscopy. *Geochim. Cosmochim. Acta* **75**, 2336-
713 2355.

714 Niles P. B., Catling D. C., Berger G., Chassefière E., Ehlmann B. L., Michalski J. R., Morris R.,
715 Ruff S. W. and Sutter B. (2013) Geochemistry of carbonates on Mars: implications for climate
716 history and nature of aqueous environments. *Space Scie. Rev.* **174**, 301-328.

717 Niles P. B. and Michalski J. (2009) Meridiani Planum sediments on Mars formed through
718 weathering in massive ice deposits. *Nat. Geosci.* **2**, 215-220.

719 Oelkers E. H. (2001) General kinetic description of multioxide silicate mineral and glass
720 dissolution. *Geochim. Cosmochim. Acta* **65**, 3703-3719.

721 Peretyazhko T., Sutter B., Morris R., Agresti D., Le L. and Ming D. (2016) Fe/Mg smectite
722 formation under acidic conditions on early Mars. *Geochim. Cosmochim. Acta* **173**, 37-49.

723 Poulet F., Bibring J.-P., Mustard J., Gendrin A., Mangold N., Langevin Y., Arvidson R., Gondet
724 B., Gomez C. and Berthé M. (2005) Phyllosilicates on Mars and implications for early Martian
725 climate. *Nature* **438**, 623-627.

726 Poulet F., Mangold N., Loizeau D., Bibring J.-P., Langevin Y., Michalski J. and Gondet B.
727 (2008) Abundance of minerals in the phyllosilicate-rich units on Mars. *Astron.Astrophys.* **487**,
728 L41-L44.

729 Rampe E. B., Ming D. W., Blake D. F., Bristow T. F., Chipera S. J., Grotzinger J. P., Morris R.
730 V., Morrison S. M., Vaniman D. T., Yen A. S. and et al (2017) Mineralogy of an ancient
731 lacustrine mudstone succession from the Murray formation, Gale
732 crater, Mars. *Earth. Planet. Sci. Lett.* **471,** 172-185.

733 Righter K., Pando K. and Danielson L. (2009) Experimental evidence for sulfur-rich martian
734 magmas: Implications for volcanism and surficial sulfur sources. *Earth. Planet. Sci. Lett.* **288**,
735 235-243.

736 Seyfried W., Shanks W. and Dibble W. (1978) Clay mineral formation in DSDP Leg 34 basalt.
737 *Earth. Planet. Sci. Lett.* **41**, 265-276.

738 Solomon S. C., Aharonson O., Aurnou J. M., Banerdt W. B., Carr M. H., Dombard A. J., Frey H.
739 V., Golombek M. P., Hauck S. A. and Head J. W. (2005) New perspectives on ancient Mars.
740 *Science* **307**, 1214-1220.

741 Story S., Bowen B. B., Benison K. C. and Schulze D. G. (2010) Authigenic phyllosilicates in
742 modern acid saline lake sediments and implications for Mars. *J. Geophys. Res. Planets* **115**.

743 Tosca N. J., McLennan S. M., Dyar M. D., Sklute E. C. and Michel F. M. (2008) Fe oxidation
744 processes at Meridiani Planum and implications for secondary Fe mineralogy on Mars. *J.*
745 *Geophys. Res. Planets* **113**.

746 Treiman A. H., Morris R. V., Agresti D. G., Graff T. G., Achilles C. N., Rampe E. B., Bristow T.
747 F., Blake D. F., Vaniman D. T. and Bish D. L. (2014) Ferrian saponite from the Santa Monica
748 Mountains (California, USA, Earth): Characterization as an analog for clay minerals on Mars
749 with application to Yellowknife Bay in Gale Crater. *Am. Mineral.* **99**, 2234-2250.

750 Vaniman D., Bish D., Ming D., Bristow T., Morris R., Blake D., Chipera S., Morrison S.,
751 Treiman A. and Rampe E. (2014) Mineralogy of a mudstone at Yellowknife Bay, Gale crater,
752 Mars. *Science* **343**, 1243480.

753 Whittig L. D. and Allardice W. R. (1986) X-ray diffraction techniques, In: *Methods of soil*
754 *analysis. Part 1 Physical and mineralogical methods* (ed. A. Klute). American Society of
755 Agronomy, Madison, pp. 331-363.

756 Wray J., Milliken R., Dundas C., Swayze G., Andrews-Hanna J., Baldridge A., Chojnacki M.,
757 Bishop J., Ehlmann B. and Murchie S. L. (2011) Columbus crater and other possible
758 groundwater-fed paleolakes of Terra Sirenum, Mars. *J. Geophys. Res. Planets* **116**.

759 Wray J. J., Murchie S. L., Bishop J. L., Ehlmann B. L., Milliken R. E., Wilhelm M. B., Seelos K.
760 D. and Chojnacki M. (2016) Orbital evidence for more widespread carbonate-bearing rocks on
761 Mars. *J. Geophys. Res. Planets* **121**, 652-677.

762 Zolotov M. Y. and Mironenko M. V. (2007) Timing of acid weathering on Mars: A
763 kinetic-thermodynamic assessment. *J. Geophys. Res. Planets* **112**.

764 Zolotov M. Y. and Mironenko M. V. (2016) Chemical models for martian weathering profiles:
765 Insights into formation of layered phyllosilicate and sulfate deposits. *Icarus* **275**, 203-220.

766

767

768

Table 1. Phases determined in the 14d-incubated Adirondack basalt simulants by XRD and Mössbauer spectroscopy. Olivine and chromite are unaltered phases from the original basalt simulant.

pH_{14d}	Crystalline phases
1.81 ± 0.01	anhydrite, natroalunite, hematite[a], chromite
2.19 ± 0.01	anhydrite, chromite
3.12 ± 0.03	dioctahedral smectite, anhydrite, hematite, olivine, chromite
3.72 ± 0.34	saponite, anhydrite, hematite, olivine, chromite
7.17 ± 0.38	saponite, anhydrite, olivine, chromite
8.38 ± 0.20	saponite, anhydrite, hematite, olivine, chromite

[a]Hematite was detected by both XRD and Mössbauer in the pH_{14d} 1.8 sample and by Mössbauer spectroscopy alone in the other samples. Hematite was present within the pH_{14d} range from 1.8 to 8.4 and likely precipitated in the pH_{14d} 2.2 and 7.2 samples not analyzed by Mössbauer spectroscopy.

Table 2. Smectite characterization data obtained by XRD and VNIR.

pH_{14d}	Smectite	XRD d-spacing, Å		VNIR combination band position, µm		
		02*l*	060	Al(Fe(III), Fe(II), Mg)OH[b]	(Mg, Fe(II), Fe(III))$_3$OH[b]	(Mg, Fe(II), Fe(III))$_3$OH[c]
3.12 ± 0.03	dioctahedral smectite	4.48	1.50	nd[a]	nd	nd
3.72 ± 0.34	saponite	4.55	1.53	2.239	2.319	nd
7.17 ± 0.38	saponite	4.58	1.53	2.246	2.319	2.403
8.38 ± 0.20	saponite	4.57	1.53	2.243	2.300	2.408

[a] nd-not detected; [b] Combination stretching and bending vibration (Neumann et al., 2011; Treiman et al., 2014); [c] Combination stretching and translation vibration (Frost et al., 2002; Chemtob et al., 2015).

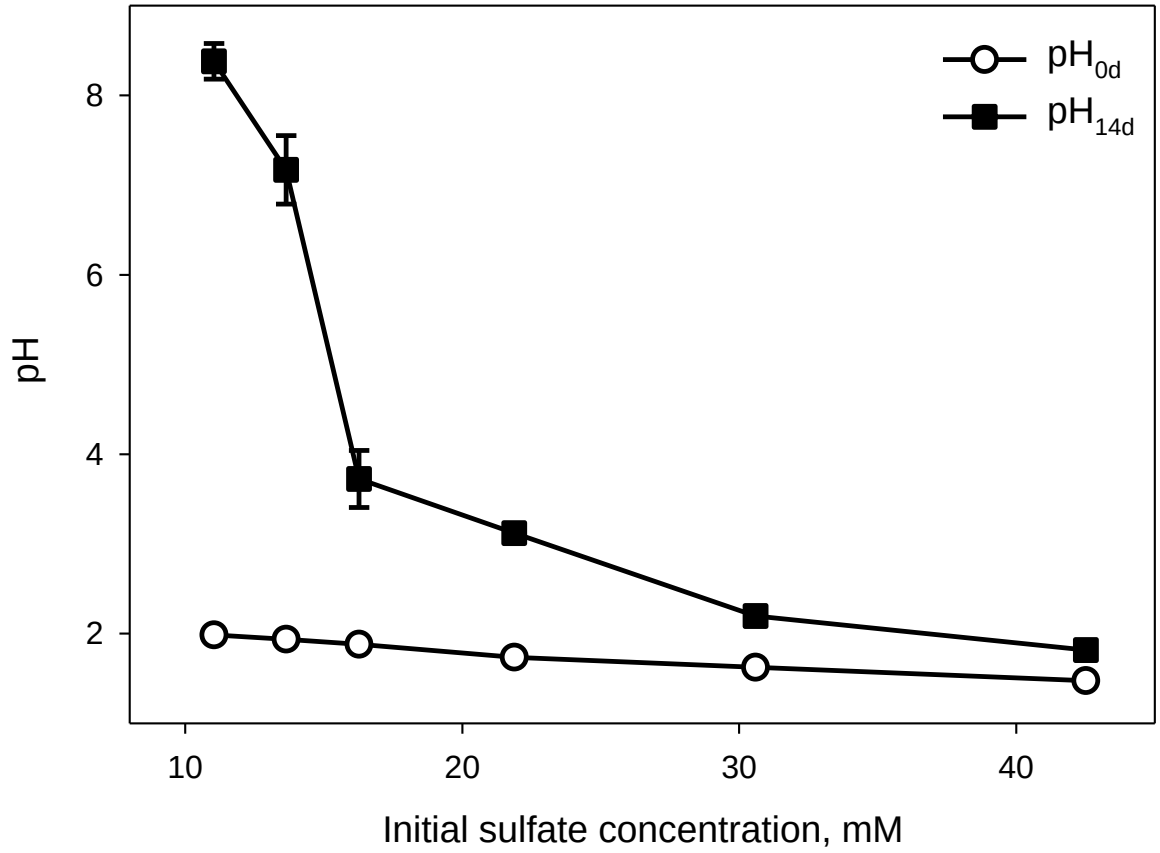

Figure 1. Initial (pH_{0d}) and final (pH_{14d}) pH in Adirondack basalt simulant suspensions as a function of initial sulfate concentrations.

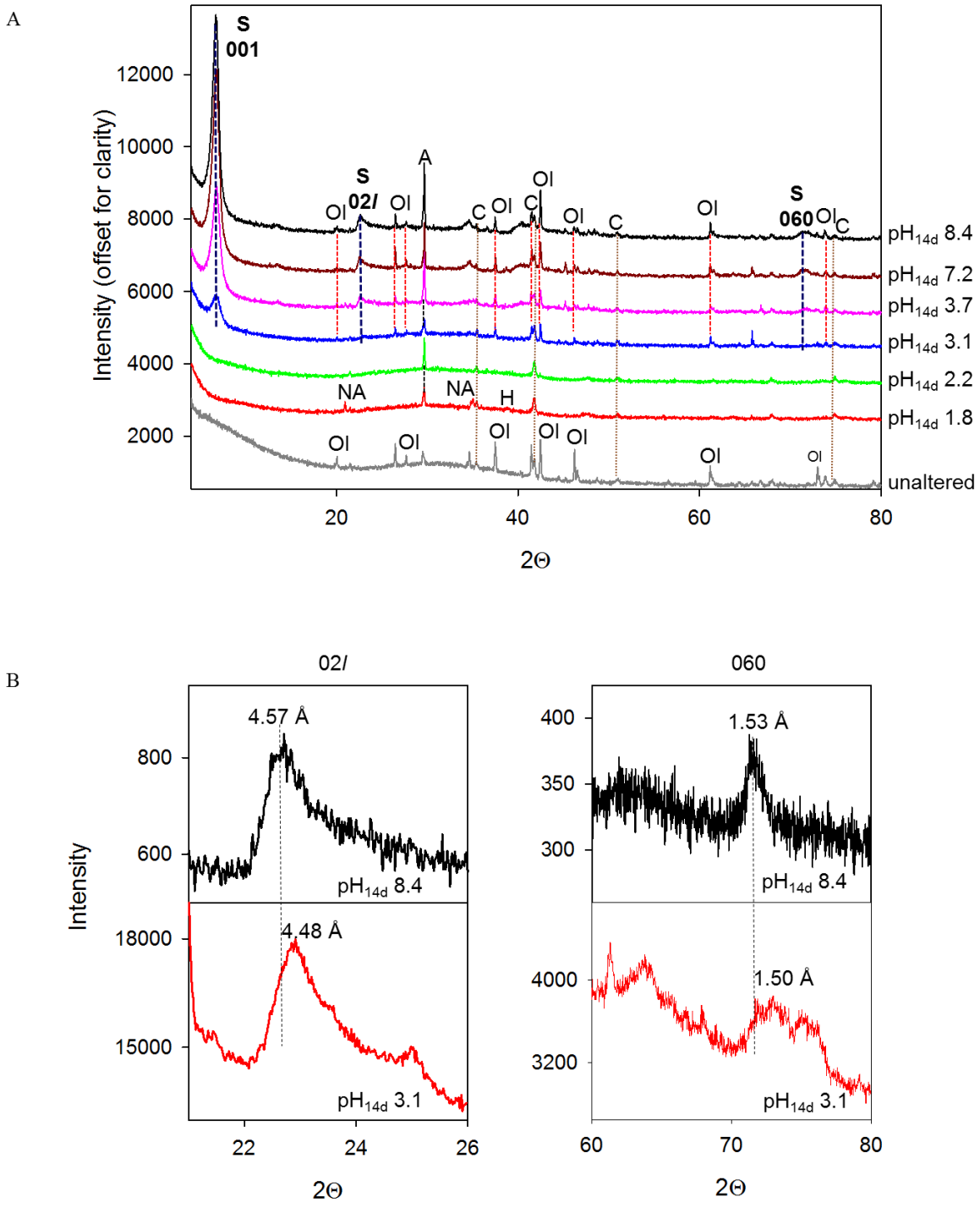

Figure 2. (a) XRD for unaltered and 14d-incubated Adirondack basalt simulant samples with different pH_{14d}. S = smectite (001, 02*l* and 060 diffraction peaks are marked next to or above the peaks), A = anhydrite, Ol = olivine, C = chromite, NA = natroalunite, H = hematite; (b) 02*l* and 060 diffraction bands for clay fractions separated from the pH_{14d} 8.4 and 3.1 samples. The bands were analyzed with a 0.02° 2θ step for 1 min and 0.02° 2θ step for 17 min in the pH_{14d} 8.4 and 3.1 clay fractions, respectively.

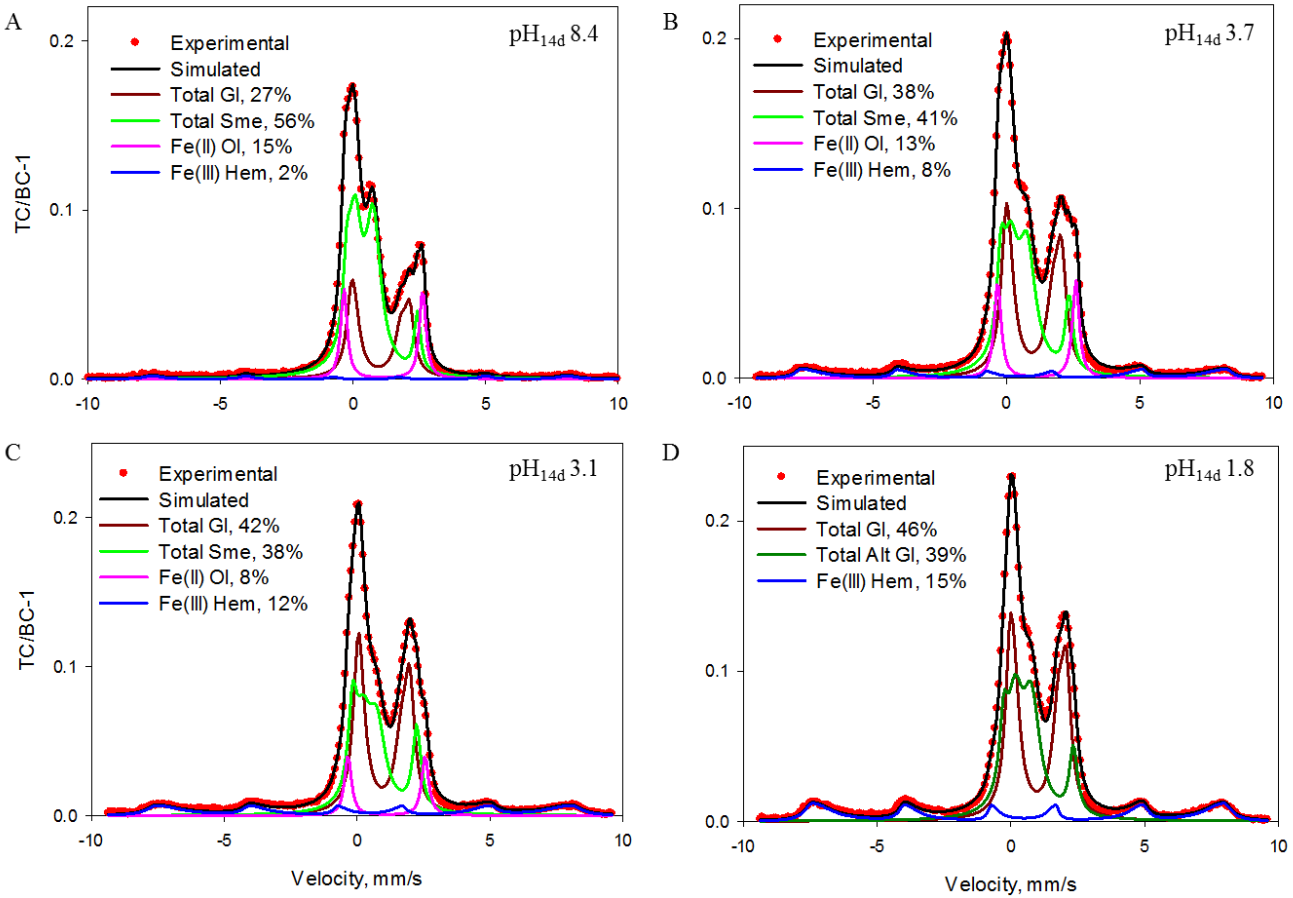

Figure 3. Mössbauer spectra and fit subspectra for 14d-incubated (a) pH_{14d} 8.4, (b) pH_{14d} 3.7, (c) pH_{14d} 3.1 and (d) pH_{14d} 1.8 Adirondack basalt simulant collected at RT [subspectral areas in % are for Ol = olivine; Total Gl = total glass, a sum of 2D1 and 2D2 doublets (Table EA-2), Total Sme = total smectite, and Total Alt Gl = total altered glass, a sum of 3D2 and 2D4 doublets (Table EA-2)]. TC = total counts, BC = baseline counts.

A

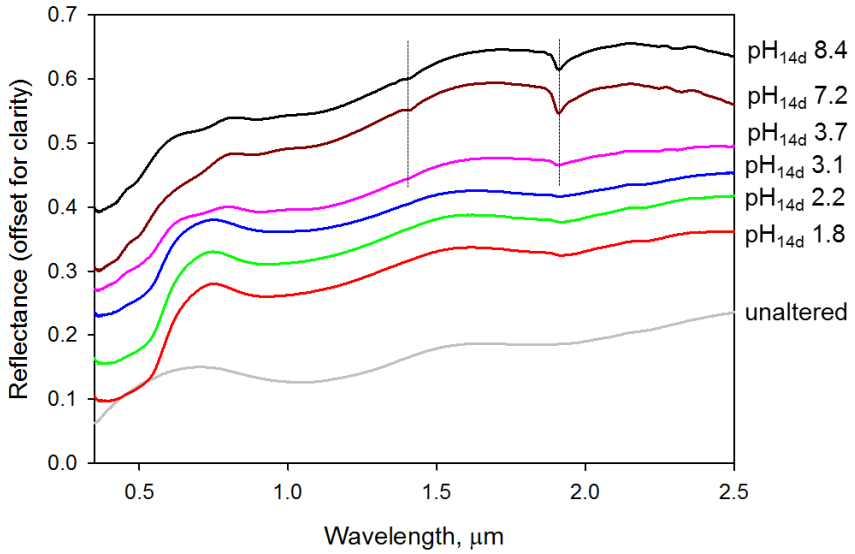

B

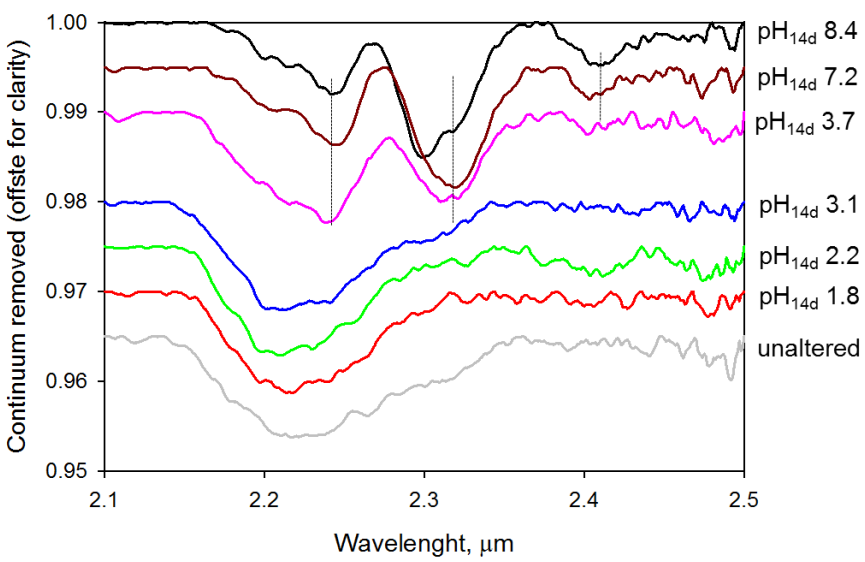

Figure 4. (a) VNIR reflectance spectra of unaltered and 14d-incubated Adirondack basalt simulant samples with different pH_{14d}. Bands at 1.4 and 1.9 µm in the saponite-containing pH_{14d} 8.4, 7.2 and 3.7 samples are marked with dotted lines. (b) 2-2.5 µm range of continuum removed reflectance spectra. Positions of M_3-OH and M_2-OH combination bands in the saponite-containing samples are marked with dotted lines (M is any combination of Al, Mg, Fe(II) and Fe(III) as octahedral cations). Characteristic Al_2OH band of montmorillonite at 2.21 µm in the pH_{14d} 3.1 sample was not detected.

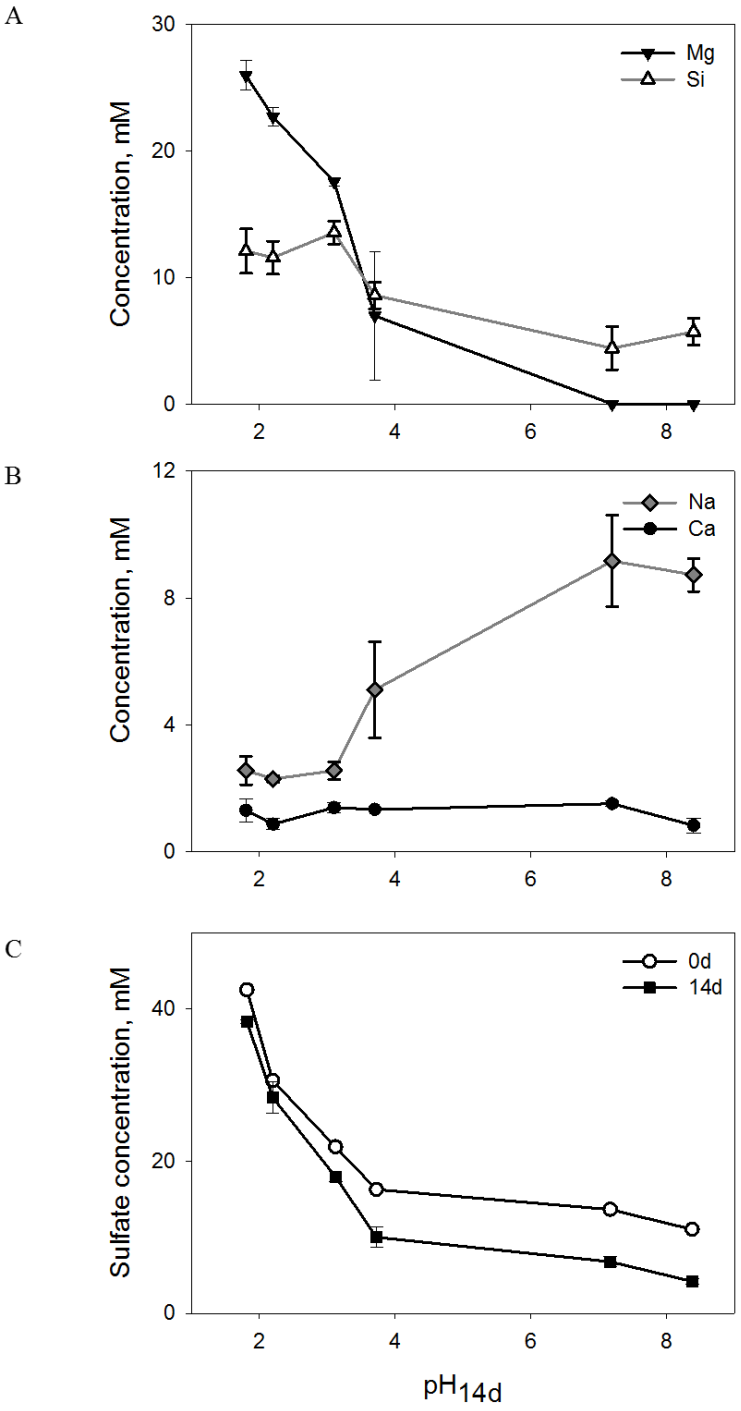

Figure 5. Concentrations of dissolved (a) Mg and Si, (b) Na and Ca and (c) sulfate in Adirondack basalt simulant suspensions as a function of pH_{14d}.

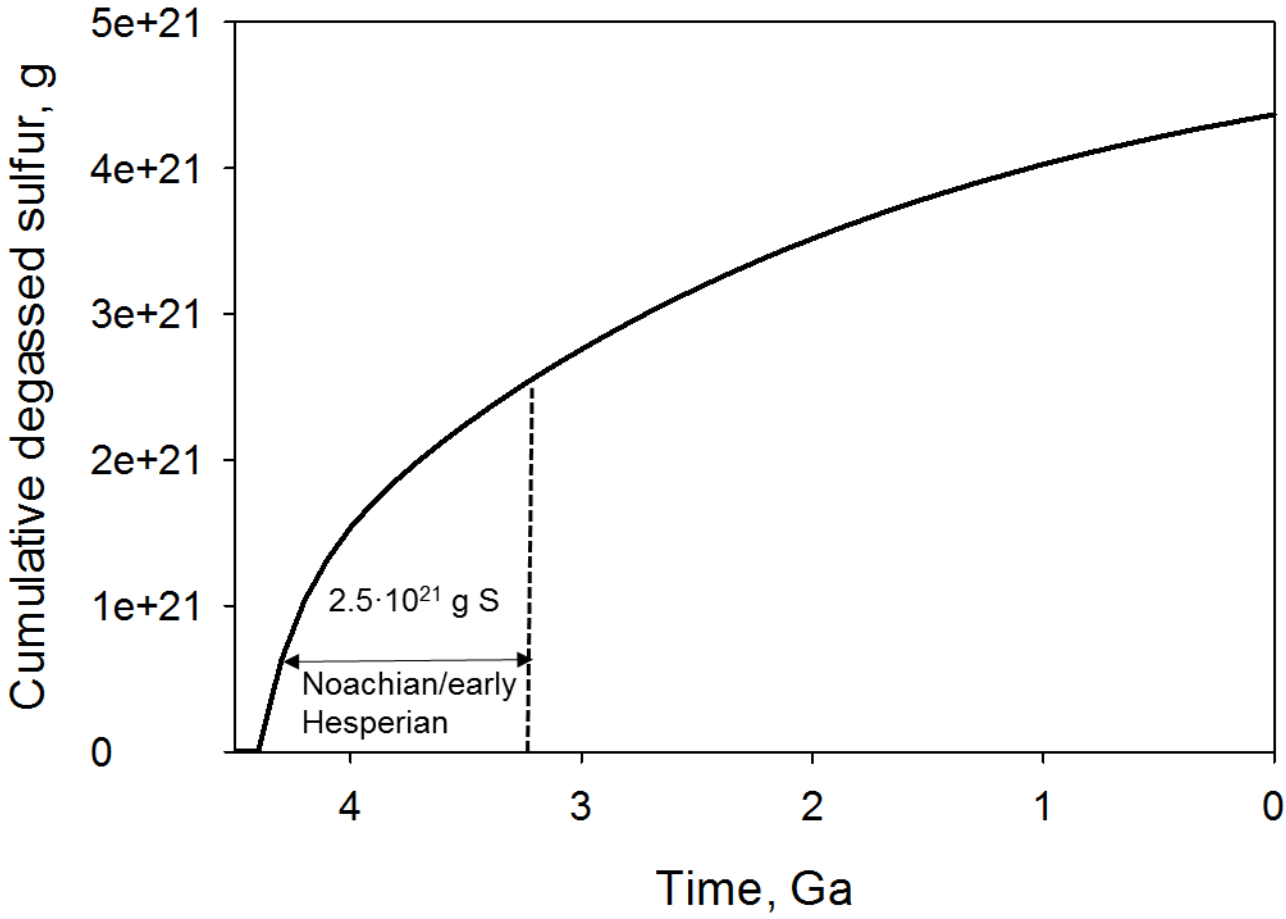

Figure 6. Sulfur degassed on Mars from 4.5 Ga to present calculated using the crust production model (eq. 2, Hirschmann and Withers 2008) and amount of sulfur degassed from 1 kg magma (2400 mg/kg, Righter et al., 2009). The calculated total degassed sulfur from 4.5 Ga to present was $4.4 \cdot 10^{21}$ g and within the range of estimates of total sulfur release on Mars: $2.2 \cdot 10^{22}$ g (McLennan, 2012), $5.4 \cdot 10^{21}$ g (Gaillard and Scaillet, 2009), $1.7 \cdot 10^{20}$ g (Craddock and Greeley, 2009) and $4.5 \cdot 10^{19}$ g (Righter et al., 2009). Dashed line shows a boundary between early and late Hesperian.